SHEAR VELOCITY AND INTRINSIC ATTENUATION VARIATIONS WITHIN THE AEGEAN LITHOSPHERE DEDUCED FROM SURFACE WAVES

I. Kassaras[1], F. Louis[1], K. Makropoulos[1], A. Magganas[2]

[1]National and Kapodistrian University of Athens, Faculty of Geology and Geoenvironment, Department of Geophysics-Geothermics,, Panepistimioupolis, Zografou, Athens 15784, kassaras@geol.uoa.gr
[2]National and Kapodistrian University of Athens, Faculty of Geology and Geoenvironment, Department of Mineralogy & Petrology, Panepistimioupolis, Zografou, Athens 15784, amagganas@geol.uoa.gr

ABSTRACT

Towards contributing to the better knowledge of the Aegean lithosphere we introduce experimental elastic and anelastic parameters by analyzing more than 1100 long period Rayleigh waves seismograms. The wavetrains were recorded at the broadband stations installed some years ago in the Aegean region for the SEISFAULTGREECE project. Path-average phase velocities and attenuation coefficients of fundamental Rayleigh waves crossing the Aegean were extracted over the period range 10-100 s. This is the first time that anelastic parameters of the long period wavefield are determined for the region.

By stochastic inversion 36 path-average models of shear velocity and 19 path-average models of inverse shear Q were derived down to 200 km. Furthermore, the 1-D path-average models were combined in a continuous regionalization tomographic scheme and a 3-D model of shear velocity variation and a 3-D model of inverse shear Q variation down to 120 km were developed. In the tomograms prominent is a low shear velocity/high attenuation zone in the back-arc region, especially in the central and north Aegean. This zone is associated with an area with high extensional strain rates due to the westward propagation of the NAF system within the Aegean, slab roll back and back arc basin development. The observed pattern suggests a hot or perhaps partially molten uppermost asthenospheric mantle or distributed deformation of the upper mantle beneath this region, or a combination of both, that is an uppermost mantle with high-stress deformation zones associated with faulting and fluid induced magma generation.

A high velocity/low attenuation zone is evident in South Aegean and continental Greece indicating the subducted African lithosphere beneath the Aegean. The precise shape and position of the slab cannot be resolved by the data used in the present study because of insufficient lateral resolution in the specific areas.

SHEAR VELOCITIES

Purpose of the study

The advancement of a previously constructed 3-D shear velocity model of the upper mantle beneath the Aegean. Averaged 36 1-D path average shear velocity models were determined. Now, this dataset is combined in a continuous regionalization tomographic scheme, to derive a smooth model of lateral shear velocity variations and a qualitative estimation of the model constraint as a function of geographical position.

Data-Methodology

Phase velocities of the fundamental mode of Rayleigh wave propagating across the Aegean were used.

Approximately 430 teleseismic earthquakes with M>5, recorded during by 12 broadband stations were considered. Data from 3 GEOFON stations in south Aegean were also used.

Waveforms of 386 events with epicentral distances larger than 30^0 characterized by satisfactory signal-to-noise ratio were analyzed.

Phase velocity dispersion curves of the fundamental mode Rayleigh waves were determined by the two-station technique for periods 10-100 sec along 36 interstation pathways covering the Aegean region.

The inversion of the path-average dispersion curves yielded 18 shear velocity models down to 200 km depth and 18 models down to 120 km depth.

Only layers between 30-120 km depth were employed in the tomographic scheme, to ensure a homogeneous sampling of the study area.

The SEISFAULTGREECE PROJECT

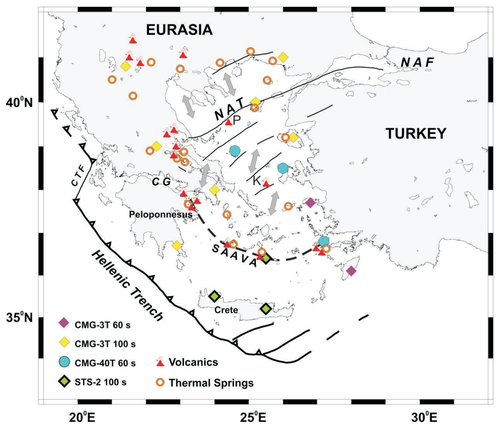

Figure 1. Map showing the location of the stations used in the present study, main active tectonic features of the Aegean after Armijo et al. (1999), Pliocene to Recent volcanic centers and main thermal springs. Abbreviations for geographical names: CG = Corinth Gulf; NAT = North Aegean Trough; NAF = North Anatolian Fault; SAAVA = South Aegean Active Volcanic Arc; CTF = Cephalonia Transform Fault; P = Psathoura; K = Kalogeri.

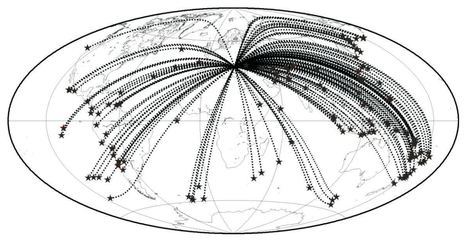

Figure 2. The 176 used teleseismic events and propagation great circles.

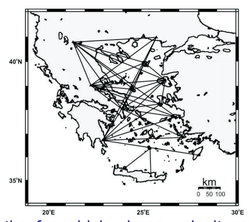

Figure 3. Paths for which phase velocity measurements were obtained.

RESOLUTION ASSESSMENT

1. Null Space Energy indicator (NSE).

An estimate of the local reliability in model space.High values of NSE indicate solution vagueness. The largest uncertainties occur at the lower boundaries of the two models and especially in the second case (figure 4B) as a direct effect of limited ray coverage. NSE is quite low while in some areas it's almost zero (North East part of figure 4).

2. Resolution Matrix

The upper left pixel of the model relates to the lower right diagonal element of the resolution matrix.The resolution of the central elements of the matrix (corresponding mainly in the central parts of the model) in Fig. 5 is quite high while in general the off-diagonal elements are of small amplitude This implies that the resolution for these depths is fair enough to accept most of the anomalies in the solution tomogram.

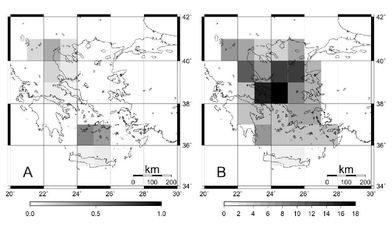

Figure 4. Null space energy (NSE) distributions (A) and the corresponding ray density map (B).

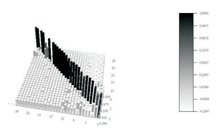

Figure 5. Perspective view of the resolution matrices at the cases of 75-120 (A) and >120

CONTINUOUS REGIONALIZATION OF PATH AVERAGE SHEAR VELOCITIES

The tomographic scheme consists of a continuous formulation of the inverse problem and the least-square criterion. The algorithm used (Debayle and Sambridge 2004) is an optimized version of the Montagner(1986) approach for continuous regionalization of surface wave path-average measurements.

The lateral smoothness of the inverted model is obtained by assuming a priori a Gaussian correlation between neighboring points with a specified scale length Lcorr and a scale factor σ(r).

L_{corr} imposes correlaLtion between points separated by distances of order orr Calculations are restricted to the pairs of points which satisfy, $D_i < 2.64\ L_{corr}$ where is the distance between geographical points.

L_{corr} was chosen equal to 150-200 km, favoring a smooth model considering the ray density and wavelengths used.

The a priori standard deviation σ(r)controls the amplitude of the perturbation allowed in the process and the horizontal correlation length is a spatial filter that constrains the lateral smoothness of the model.

The a priori standard deviation σ(r) was taken equal to 0.05 km/s, according to a conservative average phase velocity error estimate.

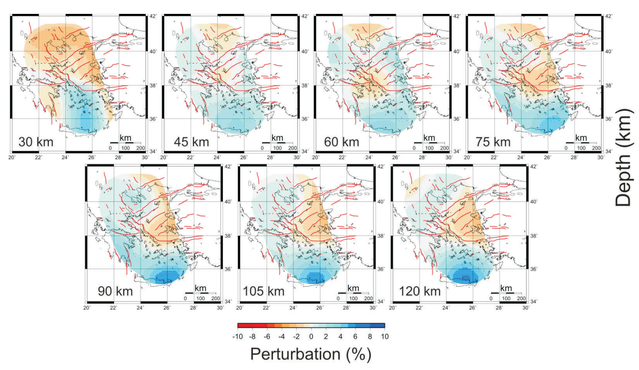

Figure 6. Tomographic slices of the shear velocity model at different depths. Tomograms start at 30 km depth. The velocity perturbations are indicated with a color scale in percent relative to a common reference model, derived from the average shear velocity at each depth. The North Anatolian Trough and other major tectonic features are superposed onto the maps.

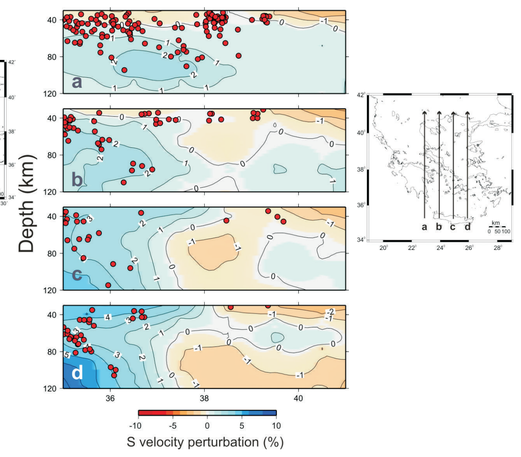

Figure 7. Vertical cross-sections across the 3-D shear wave velocity model. Velocity variations are in percentage with respect to the average shear velocity at each depth. Solid red circles represent locations of subcrustal earthquakes.

SHEAR VELOCITY VARIATIONS

The pattern of lateral shear velocity perturbations is consistent with major phase velocity anomalies for the period range 10 to 100s (Kassaras et al. 2005).

They are also consistent with shear velocity variations down to the depth of 140 km (Bourova et al. 2005).

Regarding the amplitude of S-wave velocity variations (approximately -3% to +6%), it implies a good compromise between experimental measurements and the inverted model. The amplitude of the velocity variations is in agreement with previous studies in the Agean based on local and teleseismic tomography and surface wave tomography.

At the depth of 30 km, shear velocities reflect variations of crustal thickness in the area. Our model shows a thin crust in South Aegean, while in North Aegean and continental area the crust appears thicker.

Perhaps the most dominant feature of the model is the velocity contrast in Central and North Aegean. This tendency is evident in almost the whole depth range of the model. The amplitude of the observed velocity contrast is between -1% and -3%. Vs variations of 1% to 3% over distances of a few hundred kilometers, as observed in our model, can be obtained with temperature variations of 700 to 2000 C, which may result to melts and/or fluids circulation. Moreover, Pleistocene to Recent trachyandesitic volcanism and high heat flow, as expressed by hot springs in Central Greece (SE. Thessaly and N. Evoicos Gulf), can be the result of mantle-originated magmas differentiated during their ascent through the relatively thin crust of the area. The southwestwards NAF propagation during the last 5 Ma, which has reached the eastern continental coast of Central Greece, may also be of significant importance to both volcanism and low velocity zone in this particular location.

High velocities are observed in continental Greece at depths 45-120 km. The observed high velocity zone extends from north-western Greece to the Turkish coast, going through western Greece and southern Aegean and subparaller to the Hellenic trench. We interpret this structure as the subducted lithospheric African plate, which is bounded to the east of the study area, in the region of southwestern coast of Turkey.One of the main features of our model is a high-velocity anomaly in south Aegean, associated with the slab (Figure 13). However, a limited resolution and better path coverage is required to obtain constraints on the slab geometry. The absolute shear velocities in the slab at a depth of 100 km are up to 4.70 km s^{-1} corresponding to a P velocity of 8.14 km s^{-1} (assuming a Poisson ratio of 0.25) which is in good agreement with the P velocity of 8.1 km s^{-1} obtained in the same location by Papazachos and Nolet (1997)..

North of NAT, a high velocity anomaly is observed, possibly associated with the southern margin of the Eurasian continental lithosphere. Although null space energy is high at this part of our model the pattern is compatible with a high velocity anomaly found at the same area by Papazachos and Nolet (1997).

ATTENUATION

Purpose of the study

Surface waves have been widely used to study the shear-wave velocity distribution in the Aegean. However, evident is the lack of surface wave attenuation studies, which, in contradiction to body and coda waves can provide information on the depth dependence of *Q*, inferring resources to understand the material and physical conditions in the lithosphere and upper mantle.

This work is towards contributing to the better knowledge of the deep structure of the Aegean by introducing experimental anelastic parameters via the study of long period Rayleigh waves attenuation.

Computation of attenuation coefficients

The Multiple Filter Technique (MFT) (Herrmann, 1973) was utilized for the identification of the fundamental Rayleigh waves and to extract spectral amplitudes.

After rejecting largely erroneous data, the two-station method was applied for 330 pairs of stations to obtain the attenuation coefficients (γ) in the period range 10-100 s.

Attenuation coefficient errors assessment

Several effects strongly impact surface wave amplitude, such as focusing- defocusing, departures from the great-circle path and multipathing. In order to minimize those effects and to set the tolerance range of our measurements, we performed the following procedure:

1. We employed the seismograms used by Kassaras et al. (2005), who performed a strict seismogram selection procedure when working with phase velocities computed by the two-station method.
2. We conducted a synthetic experiment adequately parameterized for our study area. By utilizing an average 1-D shear velocity model derived for the region (Kassaras et al. 2005) and perturbing Q_b we calculated the theoretical quotients (γ) for various interstation distances, relevant to the lengths of our paths.
3. To control the errors for each individual path, we tried to collect as many events for each station pair as possible, adopting only similar observations, reducing thus the standard deviations of the mean values.
4. Given that short interstation distances can cause problems when using the two-station method, measurements for short interstation distances were compared with those for longer interstation distances, and were also compared with the average values to examine the usability of the data.

As expected, given the strong impact of the above mentioned effects, the largest part of the analyzed dataset exceeded the tolerance range and was consequently rejected.

In conclusion, we adopted 75 interstation attenuation coefficient curves as representative of 17 paths across the Aegean and calculated the average value and the corresponding standard deviation of γ_R for each period and each path.

The tomographic scheme used is a revised version of the Montagner (1986) approach for continuous regionalization of surface wave path-average measurements.

L_{corr} was chosen equal to 150 km, favouring a smooth model considering the ray density and wavelengths used.

$\sigma(r)$ was taken equal to 0.5×10^{-3} km^{-1}, according to a conservative attenuation coefficient error estimate.

The 17 attenuation coefficient curves obtained were combined over a 1×1 degree grid into a 3-D model for the lateral variations of attenuation. The period range of the computed tomograms was restricted between 10 and 60 s, since the poor path coverage beyond 60 s (8 paths) did not allow for efficient results.

Using Voronoi diagrams to assess model constraint

Due to the irregular path coverage of the region we used Voronoi polyhedra to estimate the variation of the model constraint as a function of geographical position.

As a starting point we built an initial Voronoi diagram falling on a 2° × 2° grid.

From this starting Voronoi diagram we proceeded iteratively by building new diagrams in such a way that a particular quality criterion depending on the paths distribution is satisfied for each cell.

In the final optimized diagram each cell denotes the size of the structures our inversion can model.

Best resolution is achieved in central and north Aegean. In northern Greece and south Aegean, resolution is not sufficient, but it is better in the E-W direction.

Continuous regionalization of path-average Q_b^{-1}

The path-average 1-D Q_b^{-1} models with depth obtained by the inversion of attenuation coefficient curves were empolyed to the continuous regionalization scheme in order to obtain local Q_b^{-1}.

- L_{corr} was chosen equal to 150 km.
- $\sigma(r)$ was taken equal to 5×10^{-3}.

17 path-average 1-D Q_b^{-1} models with depth were combined over a 1×1 degree grid into a 3-D model for the lateral variations of Q_b^{-1}. The depth range of the computed tomograms was restricted between 30 and 120 km.

Q_b^{-1} tomograms

Resolution of the anelastic model, assessed by optimized Voronoi polyhedra, is limited, as a consequence of the reduced ray coverage causing a considerable blurring at the final tomograms. However, anelastic tomograms are compatible with shear velocity variations. Hence, even though Q models derived from surface wave attenuation data may have large uncertainties, we are still be able to obtain information about the variability of Q and its relation to crustal and upper mantle structure and evolution.

Except in the case of 30 km depth, where elastic tomography is highly connected with crustal thickness, high attenuation is associated with low shear velocities, apparently in the North Aegean region. As in elastic tomography this region is about 200 km wide and extends in depth possibly deeper than our model. The presence of this zone could be attributed to several reasons, including melting in the asthenosphere and distributed deformation. Indeed, the NAF in the area and the associated intense north-south extension caused rapid tectonic instability in the area expressed in both mantle and crustal levels. NAT and Orfanos Gulf basins are their crustal surface results. NE-SW mantle olivine anisotropy [19] and extension in about the same direction suggest upper mantle deformation or flow. Recent magmatic mantle processes are manifested in the small volcanic islets of Psathura and Kalogeri of Northern and Central Aegean, respectively. They consist of sodic basalts derived from oceanic island basalt (OIB) asthenospheric mantle source similar in geochemical character to Pliocene basalts of Western and Central Anatolia. Presumably, most magma remains below the crust, underplating it, as indicated by the high attenuation mantle zone depicted clearly in the northern part of the cross sections of Figure 15. High heat flow in the area of N. Aegean signified by many hot springs in its islands, as well as the above mentioned petrogenetic and tectonic processes, may be related with a relatively thin crust (<28 km) or strong delamination, that is a very thin to totally absent lithospheric mantle in the area.

At 30 km depth, the high attenuation anomaly could be associated with thermal activity from hot fluids residing in deep crustal to shallow mantle levels below the South Aegean active volcanic centers, due to dehydration and delamination processes within the African subducted slab. Deeper than 30 km, the high attenuation anomalies are restricted beneath North Aegean. Low attenuation is now observed throughout the Hellenic mainland likely attributed to subducted features.

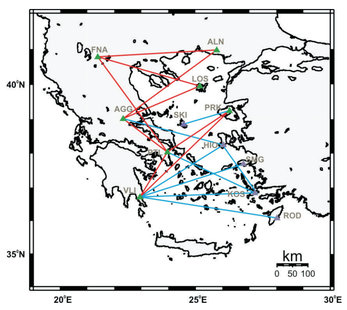

Figure 8. Paths for which attenuation coefficient measurements were obtained. (Red): paths sampled up to 100 s. (Blue): paths sampled up to 60 s.

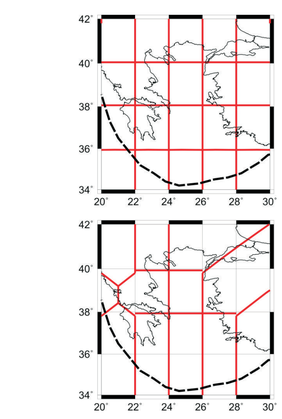

Figure 9. Voronoi diagrams (red cells) ro assess the model constraint as a function of geographical position. Top: Initial Voronoi diagram over a 2° × 2° grid. Bottom: Optimized Voronoi diagram.

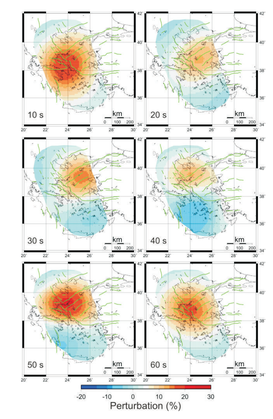

Figure 10. Attenuation coefficient maps are shown for 6 periods varying from 10 to 60 s. Attenuation variations are relative to the average attenuation coefficient at each period.

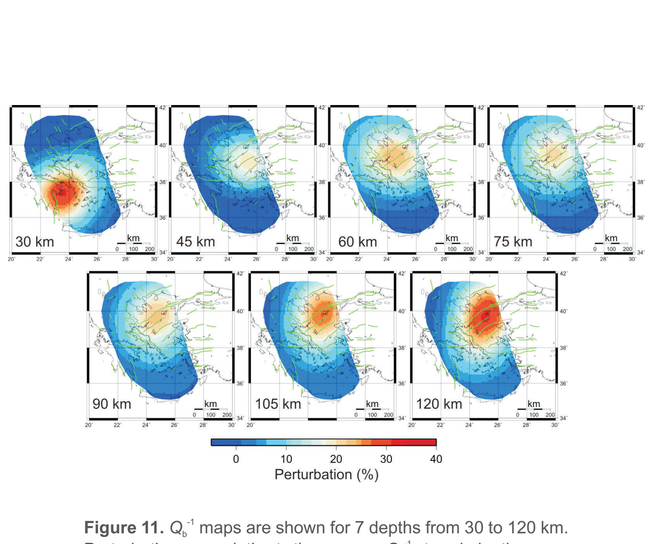

Figure 11. Q_b^{-1} maps are shown for 7 depths from 30 to 120 km. Perturbations are relative to the average Q_b^{-1} at each depth.

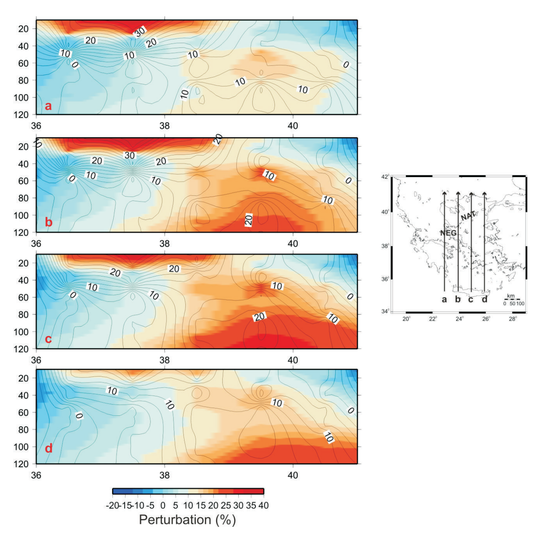

Figure 12. Cross-sections across the Q_b^{-1} model.

CONCLUSIONS

From the study of tomographic schemes of path-average phase velocities and attenuation coefficients of fundamental Rayleigh wave crossing the Aegean a 3-D model of shear velocity variation and a 3-D model of Qb-1 variation down to 120 km were obtained.

The most prominent features in the tomograms are:

1) A low shear velocity zone in central and north Aegean, which correlates well with the derived anelastic tomograms which present high attenuation in this area. This low velocities/high attenuation zone, which indicates the lithosphere-asthenosphere boundary occurs at depths less than 120 km beneath the area, could be attributed to:
   i) High extensional strain rates related with the NAF system within the Aegean, slab roll back and distributed deformation of the upper mantle, and/or
   ii) A hot or most probably partially molten lithosheric and uppermost asthenospheric mantle, which generates subordinate Pleistocene to Recent volcanism and high heat flow in the area.
2) A high velocity/low attenuation zone in the southern part of the study area and deeper than 30 km indicating the cool subducted African lithosphere beneath the South Aegean.
3) A high attenuation zone observed in the South Aegean at about 30 km depth that probably corresponds to serpentinization, hot fluids and/or magma batches residing in deep crustal to lithospheric mantle wedge levels.
4) A low attenuation region throughout the Hellenic mainland at crustal depths, which is likely ascribed to the subducted slab.